

# A General Theory of Temporal Connectivity

Keith Smith<sup>1,2,\*</sup>, Loukianos Spyrou<sup>1</sup>, & Javier Escudero<sup>1</sup>

## Abstract

Methods to analyse the pair-wise connectivity of data in the temporal domain can provide a rich framework with which to extract transient, dynamic information. This paper presents a theoretical framework for a novel and highly flexible method to this end. By constructing a graph encoding the topology of connectivity, we expound upon a general theory for graph functions which allow for novel temporal probing of the connectivity information, defined as ‘temporal connectivity’. This includes methods to compute a special form of classical network measures at the temporal resolution of the signal. We present appropriate solutions of functions for three pertinent connectivity metrics- correlation, coherence and the phase-lag index- and show the usefulness of this approach in simulations of the Kuramoto model and in detecting spheroids in a noisy 3D grid. We apply our methods to examples of international trade and EEG brain functional connectivity. In the former, we reveal important insights into the effectiveness of integration in global economics. In the latter, we show that our approach combines signal dynamics and functional connectivity in a powerful way, outperforming either method on its own in the detection of functional differences between eyes open and eyes closed resting states. This opens up a whole new way to analyse temporal information of networks which is conducive to precisely answering research hypotheses and gathering novel insights based both on the connectivity and transient temporal dynamics of the data.

## I. INTRODUCTION

Classical graph theory and network science provides a well tried and tested model for analysing topologies of weighted edges derived from interactions, similarity, connectivity or distances between the agents, recordings or information received at different points of a given space [1], [2]. Analysing networks of data in the temporal domain is hampered by the static nature of the constructed network. A considerable contingent of research solutions for temporal network analysis [3] relies on constructing a number of distinct chronologically separated graphs and forming a multi-layered structure [4]. This approach, however, is limited by sampling rates- the less samples used to define the network, the less reliable is the connectivity estimate. We propose an approach named ‘temporal connectivity’ which can act either as an alternative, or a complementary analysis to overcome these limitations and more generally provide an elegant and highly flexible temporal network analysis which can emphasise important signal dynamics.

The theory introduced generalises the Modular Dirichlet Energy (MDE) method found in [5] to a general approach for temporo-topological analysis of multivariate signals. Particularly this generalises to the use of various connectivity metrics and various related temporal connectivity functions. This theory stems from Graph Signal Processing (GSP) [6] [7], a recently developed theoretical branch which aims to gain new and important insights of graph models in which there is an intrinsic value associated with each vertex in the graph. Our approach looks at the framework of GSP from a new perspective, focused on allowing the user to tailor weighted-vertex graph analysis to answer their specific questions in a readily interpretable manner. Although problems relating to vertex-weighted graphs are known in mathematics, e.g. [8], they have scarcely been exploited for topological analysis of real world applications. GSP, on the other hand, has so far mainly been concerned with the development of a cohesive signal processing theory for graph signals, analogous to classical signal processing [6]. In applications, the focus has been on spectral graph techniques concerning the Eigen-decomposition of either the graph adjacency matrix or its Laplacian [9], [11]. However, such applications are often difficult to interpret in a meaningful way since the dimensional information of the data is jeopardised. Recent work on the integration of the temporal domain within the GSP framework is underway [10], but, this differs in that it takes a spectral approach and does not take into account complex signal interactions on the graph signal.

<sup>1</sup>Institute for Digital Communications, School of Engineering, University of Edinburgh, West Mains Rd, Edinburgh, EH9 3FB, UK

<sup>2</sup>Alzheimer Scotland Dementia Research Centre, Psychology Department, University of Edinburgh, 7 George Square, Edinburgh, EH8 9JZ, UK

\*PhD funded by EPSRC, e-mail: k.smith@ed.ac.uk

The theoretical framework set out brings the theory of multivariate signal analysis, graph signal processing and network science into a single setting. Using this framework, the theory of temporal connectivity emerges naturally. Essentially, temporal connectivity is the product of graph connectivity with an appropriately defined temporal function which allows, depending on the application or perspective, for the temporal probing of the connectivity information or connectivity-based filtering of pair-wise signal dynamics. Particularly, we provide reasonable solutions for frequency and phase-based connectivity in the form of coherence and phase-lag index, respectively. Our main aims here are thus to introduce the general theoretical setting for computing temporal connectivity (section II) and, in testing, to provide evidence for the benefits of this theory over a benchmark multilayer network approach [4] on which temporal network analysis [3], [12] currently relies. For this, we use simulations of the Kuramoto model (sections III & IV A) and a spheroid travelling on a 3D grid (sections III & IV B) and test the method on real applications (sections III & IV C) in determining integrated actors in global economics and activated brain regions in neurophysiology.

These techniques thus hold wide ranging consequences for the temporal analysis of networks including in functional brain networks [13], [14], economic networks [15] and, indeed, in every topic in which temporal information of networks is important [3].

## II. PROPOSED THEORETICAL FRAMEWORK

### A. Background

1) *Multivariate Signals*: Let  $\mathbf{X} \in \mathbb{R}^{n \times p}$  be a multivariate signal with  $n$  channels  $\mathbf{X} = [\mathbf{x}_1, \dots, \mathbf{x}_n]^T$ , located in a Euclidean space at points  $[\mathbf{d}_1, \dots, \mathbf{d}_n] \subset \mathbb{R}^{n \times m}$ , respectively, where each  $\mathbf{x}_i$  is a  $1 \times p$  vector. Let  $T = [t_0, t_\infty]$  be an epoch of interest of the signal and let  $t \in T$  such that  $x_i(t)$  is the sample of channel  $\mathbf{x}_i$  at time  $t$ . Further, we define  $\mathbf{v} \subset \{1, \dots, n\}$  as a subset of channels of interest so that  $\mathbf{X}(\mathbf{v}, T)$  is a temporo-spatial subspace of  $\mathbf{X}$ .

The analytic signal of  $\mathbf{X}$  is defined as

$$\hat{\mathbf{X}} = [\hat{\mathbf{x}}_1, \dots, \hat{\mathbf{x}}_n] \in \mathbb{C}^{n \times p}, \quad (1)$$

where each  $\hat{\mathbf{x}}_i = \mathbf{x}_i + i\tilde{\mathbf{x}}_i$ , where  $\tilde{\mathbf{x}}_i$  is the Hilbert transform of  $\mathbf{x}_i$ .

2) *Connectivity analysis*: We define some function of connectivity,  $F$ , of pairwise channels,  $\{\hat{\mathbf{x}}_i, \hat{\mathbf{x}}_j\}$ , in  $\hat{\mathbf{X}}$  as

$$\begin{aligned} F : \quad \mathbb{C}^{2 \times p} &\rightarrow \mathbb{R} \\ \{\hat{\mathbf{x}}_i, \hat{\mathbf{x}}_j\} &\mapsto F(\hat{\mathbf{x}}_i, \hat{\mathbf{x}}_j), \end{aligned} \quad (2)$$

and we say  $F(\hat{\mathbf{X}}) = \mathbf{W} \in \mathbb{R}^{n \times n}$  such that

$$W_{ij} = \begin{cases} F(\hat{\mathbf{x}}_i, \hat{\mathbf{x}}_j), & i \neq j \\ 0, & i = j. \end{cases} \quad (3)$$

The matrix  $\mathbf{W}$  can thus be thought of as the weighted adjacency matrix of an undirected graph.

### B. General framework

We introduce the definition  $G = (\mathcal{V}, \hat{\mathbf{X}}, \mathcal{E}, \mathbf{W})$  as an undirected graph where  $\mathcal{V}$  is the set of vertices with  $|\mathcal{V}| = n$ ;  $\hat{\mathbf{X}} \in \mathbb{C}^{n, p}$  the chronologically defined, complex weights of  $\mathcal{V}$ ;  $\mathcal{E}$  the set of edges with  $|\mathcal{E}| = 2m$ ; and  $\mathbf{W} = \{w_{ij}\}_{(i,j) \in \mathcal{E}} \in \mathbb{R}^{n \times n}$  the weighted adjacency matrix corresponding to the weights of  $\mathcal{E}$ . Then  $(\mathcal{V}, \hat{\mathbf{X}})$  is the vertex space relating to a weighted vector  $\hat{\mathbf{X}}$  with elements indexed by the vertex set  $\mathcal{V}$  and  $(\mathcal{E}, \mathbf{W})$  is the edge space relating to a weighted matrix  $\mathbf{W}$  with elements indexed by the edge set  $\mathcal{E}$ . Hence,  $G$  constitutes the graph space of the combined vertex and edge spaces where vertices and edges joining those vertices are determined by the vertex labels  $\{1, \dots, n\}$ .

1) *Acting on the vertex space*: A function,  $F_{\mathcal{V}}$ , on the vertex space  $(\mathcal{V}, \hat{\mathbf{X}})$  is defined on the vertex weights as

$$\begin{aligned} F_{\mathcal{V}} : \quad \mathbb{C}^{n \times p} &\rightarrow \mathbb{C}^{m \times q} \\ \hat{\mathbf{X}} &\mapsto F_{\mathcal{V}}(\hat{\mathbf{X}}), \end{aligned} \quad (4)$$

Useful examples of such functions where  $n = m$  include permutations and thresholds. For  $n = m$  and  $p = q$ ,  $F_v$  can be a spectral filtering function. Particularly, where there is a time dimension involved, this problem reduces to one of conventional multivariate signal processing.

2) *Acting on the edge space:* Similarly, a function  $F_{\mathcal{E}}$  on the edge space  $(\mathcal{E}, \mathbf{W})$  is defined on the edge weights as

$$\begin{aligned} F_{\mathcal{E}} : \mathbb{R}^{n \times n} &\rightarrow \mathbb{R}^{m \times l} \\ \mathbf{W} &\mapsto F_{\mathcal{E}}(\mathbf{W}). \end{aligned} \quad (5)$$

Thresholds and permutations are useful considerations of such functions when  $n = m = l$ . Again, much interest is taken on functions which map to lower spaces,  $l \leq m \leq n$ . This includes spectral and algebraic graph theory. For instance, suppose we have a matrix of pairwise-connectivity from a set of signals. Of particular interest is in applications of network science- when  $m = l = 1$  we refer to  $F_{\mathcal{E}}$  as a global graph metric, such as transitivity or characteristic path length, and when  $m = n$  and  $l = 1$ , we refer to  $F_{\mathcal{E}}$  as a local graph metric, such as the local clustering coefficient or betweenness centrality.

3) *Acting on the graph space:* In the rest of this article we are concerned with actions involving both vertex and edge spaces, which for convenience we shall call actions on the ‘graph space’. That is, we consider functions,  $F_G$ , of the general form

$$\begin{aligned} F_G : \mathbb{R}^{n \times n} \times \mathbb{C}^{n \times r} &\rightarrow \mathbb{R}^{m \times l} \times \mathbb{C}^{l \times k} \\ \{\mathbf{W}, \hat{\mathbf{X}}\} &\mapsto F_G(\{\mathbf{W}, \hat{\mathbf{X}}\}). \end{aligned} \quad (6)$$

Particularly, Graph Signal Processing (GSP) acts on the graph space where  $\hat{\mathbf{X}}$  is referred to as the ‘graph signal’. Though generally this is regarded as a separate entity to the graph in GSP [6], [7], from our perspective the graph is an object which contains the graph signal i.e. the graph signal encodes weights of the vertex set in exactly the same way that the adjacency matrix encodes weights of the edge set.

Particularly of interest to us in this article, are such functions which provide temporo-topological metrics,  $\mathbf{z}$ , to provide a solution for the temporal analysis of connectivity information,  $\mathbf{W}$ . Thus we address functions of the form:

$$\begin{aligned} F_{G,T} : \mathbb{R}^{n \times n} \times \mathbb{C}^{n \times p} &\rightarrow \mathbb{R}^t \\ \{\mathbf{W}, \hat{\mathbf{X}}\} &\mapsto \mathbf{z}, \end{aligned} \quad (7)$$

where  $\mathbf{z}$  is a vector of length  $t$ - the number of epochs of interest. Note, mostly, in our case,  $\mathbf{W}$  is a function of  $\hat{\mathbf{X}}$ , and we seek to exploit this dependency to extract temporally precise connectivity information by filtering transient signal dynamics using robust long-term graph connectivity.

4) *Dimension preserving functions:* A special category of functions on the graph space are those which resolve to the dimensions of either the vertex space or the edge space, i.e. where  $m = n$  and  $l = k = 1$  and where  $m = l = n$  and  $k = 1$  in (6), respectively.

We define a vertex preserving function as a function,  $\mathcal{F}$ , which maps a graph,  $G$ , to  $\mathbb{C}^{n \times p}$ . Then the vertex space,  $\{\mathcal{V}, \mathcal{F}(G)\}$ , can be regarded as a transformed graph signal for a new graph,  $G_{\mathcal{F}}$ .

We define an edge preserving function as a function,  $F$ , which maps a graph,  $G$ , to  $\mathbb{R}^{n \times n}$  such that  $F(G)_{ij} = 0 \iff \mathbf{W}_{ij} = 0$ . Then the edge space,  $\{\mathcal{E}, F(G)\}$ , can be regarded as a transformed adjacency matrix for a new graph,  $G_F$ . Less strictly, an edge-dimension preserving function preserves only the dimensions of the edge space and not the condition that  $F(G)_{ij} = 0 \iff \mathbf{W}_{ij} = 0$ .

### C. Matrix operations on the graph space

Useful functions on the graph space can be efficiently computed using matrices. Such an implementation requires both a function encoding matrix,  $\mathbf{A}$ , and the operation with which the matrix acts, ‘ $\star$ ’, and can be expressed as  $F_{\mathbf{A}^{\star}}$ .

1) *Edge-dependent operations acting on the vertex space:* Since the inner-dimensions of the edge space and vertex space agree, the output of any edge-dimension preserving function together with the usual matrix multiplication,  $\cdot$ , provide useful operations which act on the vertex space,  $(\mathcal{V}, \hat{\mathbf{X}})$ . Examples include the weighted adjacency matrix,  $\mathbf{W}$ , and the graph Laplacian,  $\mathbf{L}$ , both of which have been proposed as the basis for constructing graph signal filters in GSP, as in [7] and [6], respectively, e.g.  $F_{\mathbf{L}} = \mathbf{L} \cdot \mathbf{X} = \mathbf{Y}$ .

2) *Vertex-dependent operations acting on the edge space*: Similarly, we seek a parallel for an output of vertex dependent functions towards operations on the edge space,  $(\mathcal{E}, \mathbf{W})$ . We propose a 3D tensor,  $\mathbf{J}$ , called a  $J$ -matrix, defined as follows:

$$J_{ij}(t) = \begin{cases} \mathcal{F}(\hat{x}_i(t), \hat{x}_j(t)), & i \neq j \\ 0, & i = j, \end{cases} \quad (8)$$

where the non-zero entries of  $\mathbf{J}$  are defined by what we call a ‘temporal connectivity function’,  $\mathcal{F}$ . To make an operation, we combine  $\mathbf{J}$  with a special operator,  $\diamond$ , defined such that, for a 3D tensor  $\mathbf{A} \in \mathbb{R}^{p \times n \times n}$ , composed of the  $p$   $n \times n$  matrices  $\{\mathbf{A}_k\}_{k=1}^p$ , and 2D matrix  $\mathbf{B} \in \mathbb{R}^{n \times n}$ ,  $\mathbf{A} \diamond \mathbf{B}$  produces the matrix where the  $k$ th column entries are the  $n$  values,  $\{\sum_j a_{kij} b_{ji}\}_{i=1}^n$ , of  $i$ th rows of  $\mathbf{A}_k$  matrix-multiplied with the  $i$ th columns of  $\mathbf{B}$ , i.e. the diagonal elements of  $\mathbf{A}_k \cdot \mathbf{B}$ . Then

$$(F_{\mathbf{J} \diamond}(\mathbf{W}))_{i,t} = (\mathbf{J} \diamond \mathbf{W})_{i,t} = \sum_{j=1}^n w_{ij} \mathcal{F}(\hat{x}_i(t), \hat{x}_j(t)), \quad (9)$$

so that the operator  $F_{\mathbf{J} \diamond}$  computes a graph filtered temporal analysis of vertex space function  $\mathcal{F}$  for each node,  $i$ . This provides the basis for computing temporal connectivity as detailed in section II-D.

3) *The middle way- signal function graphs*: Alternatively to the vertex only or edge only-dependent matrix operations, we can, of course, consider operations dependent on both vertex and edge spaces. This can be done by defining a Signal Function (SF) graph. An SF graph has a three dimensional adjacency matrix,  $\Delta$ , with weights determined by scalar outputs, at time  $t$ , provided by a graph weighted temporal connectivity function (8), that is:

$$\Delta_{ij}(t) = w_{ij} \mathcal{F}(\hat{x}_i(t), \hat{x}_j(t)), \quad (10)$$

where  $\Delta(t)$  is the (standard) two dimensional adjacency matrix of the SF graph at time  $t$ . Since this graph already employs both vertex and edge space components, we can consider these graphs either combined with  $\diamond$  and acting on the graph-independent matrices such as the identity matrix (paralleled to the vertex-dependent operations) or combined with matrix multiplication and acting on graph-independent vectors such as the unit vector (paralleled to edge-dependent operations). As we shall see, it is meaningful to also consider other entities related to the signal function graph such as its Laplacian.

Importantly, since the SF graph is composed of temporally related graphs, we can explore their topological characteristics. In classical network science, there are many methods proposed to analyse the topology of a graph by applying operations in the edge space, that is, on the edge weight matrix,  $\mathbf{W}$ . Such methods provide important insights and classifications of the interdependent relationships of the underlying objects. By taking matrix  $\bar{\Delta}$  as the absolute values of the SF graph,  $\Delta$ , we can directly apply all of these operations on the SF graph, slice by slice, allowing for the temporo-topological analysis of graph connectivity. We will demonstrate a basic example of this utilising a very basic clustering coefficient of vertex  $i$  at time  $t$ ,  $C_{\Delta}(i, t)$ , of the SF graph,  $\bar{\Delta}$ , defined for a weighted connectivity graph as:

$$C_{\Delta}(i, t) = \sum_{j,k=1}^n \bar{\Delta}_{ij}(t) \bar{\Delta}_{ik}(t) \bar{\Delta}_{jk}(t) = (\bar{\Delta}(t)^3)_{ii}. \quad (11)$$

Since network analysis is a well established, wide and varied field, we stick to a very basic example here and hope that the generalisability of the theory laid out allows the reader to easily go further in the required direction.

#### D. Temporal connectivity

We define temporal connectivity as a the output of a suitably chosen temporal connectivity function (8) weighted by a graph adjacency matrix,  $\mathbf{W}$ . That is, a function whose output is of the form

$$\mathbf{Z}(\mathbf{W}, \hat{\mathbf{X}}) = \begin{cases} w_{ij} \mathcal{F}(\hat{x}_i(t), \hat{x}_j(t)), & i \neq j \\ 0, & i = j. \end{cases} \quad (12)$$

Given that  $\mathbf{W}$  is the output of a function on the analytic signal  $\hat{\mathbf{X}}$  (2), if we choose the temporal connectivity function appropriately, it can reveal information of the significance of specific points in time of the connectivity

over which the adjacency matrix is constructed. For example, in [5] we chose a temporal connectivity function which helped to uncover the epochs which particularly explained the brain functional differences between cognitive tasks by a formulation which contrasted against the connectivity measure used. From the opposite perspective, the edge space  $(\mathcal{E}, \mathbf{W})$  acts as a filter for extracting useful information from the vertex space function,  $\mathcal{F}$ - strong connectivity implies those vertices are sharing or communicating important information consistently, thus these connections amplify the function at those vertices, whereas weak connectivity implies the opposite and suppresses the function at those vertices [5].

Here we present three vertex functions for three pertinent examples of connectivity matrices- correlation, coherence and phase-lag index.

1) *Correlation*: The correlation coefficient matrix is of the form:

$$\mathbf{W}_\rho = \begin{cases} \frac{\sum_t (x_i(t) - \bar{x}_i)(x_j(t) - \bar{x}_j)}{\sqrt{\sum_t (x_i(t) - \bar{x}_i)^2} \sqrt{\sum_t (x_j(t) - \bar{x}_j)^2}}, & i \neq j \\ 0, & i = j, \end{cases} \quad (13)$$

where  $\bar{x}_i$  is the mean of the values over time of the vertex  $i$ . For correlation, Smith et al. [5] previously presented the simple temporal connectivity function:

$$\theta(\hat{x}_i(t), \hat{x}_j(t)) = (x'_i(t) - x'_j(t))^2, \quad (14)$$

where  $x'_i(t)$  is the normalised signal over the vertex space, i.e.

$$x'_i(t) = \frac{x_i(t) - \bar{x}(t)}{\sqrt{\frac{1}{n-1} \sum_{k=1}^n (x_k(t) - \bar{x}(t))^2}}, \quad (15)$$

where  $\bar{x}(t) = \frac{1}{n} \sum_{k=1}^n x_k(t)$  is the mean over vertices of the signal at time  $t$ . Notably, the entries of the matrix may be negative which is an important principle, as noted in [5], for maintaining the anti-correlative information. Differences in amplitudes at time  $t$  reflects the amplitude dependent correlation coefficient,  $\rho$  (13), and thus  $\rho$  is a suitable filter of instantaneous information from  $\theta$  retrieved at  $t$  [5]. Note, this relates to the Dirichlet energy components of the graph signal from [6],

$$E(G) = \sum_{i,j=1}^n w_{ij} (x_i(t) - x_j(t))^2. \quad (16)$$

It is clear, however, that one would also be wise to consider a function deriving more directly from (13):

$$\rho(\hat{x}_i(t), \hat{x}_j(t)) = |(x_i(t) - \bar{x}_i)(x_j(t) - \bar{x}_j)|, \quad (17)$$

which we can understand as a measure of instantaneous correlation at the time point  $t$ . We shall apply both methods in simulations for comparison.

2) *Coherence*: The coherence of two channels is a function of frequency,  $\omega$ , and can be interpreted as a correlation of signal component at  $\omega$  of the channels:

$$C_{\mathbf{x}_i \mathbf{x}_j}(\omega) = \frac{|P_{\mathbf{x}_i \mathbf{x}_j}(\omega)|^2}{P_{\mathbf{x}_i \mathbf{x}_i}(\omega) P_{\mathbf{x}_j \mathbf{x}_j}(\omega)}, \quad (18)$$

where  $P_{\mathbf{x}_i \mathbf{x}_j}$  is the cross-spectral density function of  $\mathbf{x}_i$  and  $\mathbf{x}_j$  and  $P_{\mathbf{x}_i \mathbf{x}_i}$  and  $P_{\mathbf{x}_j \mathbf{x}_j}$  the respective power spectral density functions [16].

By regarding the analytic signal in terms of its instantaneous amplitude and phase components,  $\hat{\mathbf{x}}(t) = s_{\hat{\mathbf{x}}}(t)e^{i\phi_{\hat{\mathbf{x}}}(t)}$ , analogously with correlation, we proceed with the instantaneous amplitude as the temporal connectivity function for coherence:

$$\zeta(\hat{x}_i(t), \hat{x}_j(t)) = (s_{\hat{\mathbf{x}}_i}(t) - s_{\hat{\mathbf{x}}_j}(t))^2, \quad (19)$$

encoding the squared difference of the envelopes of the signals at frequency  $\omega$ . Coherence cannot be negative, thus it is a more straightforward case than correlation- high coherence and large differences in the instantaneous amplitudes can be taken generally as a contrast of information; whereas with a small difference in amplitudes implies agreement of information. Thus large temporal connectivity implies some notable discrepancy or epoch of interest in the given time window with the underlying long-term connectivity.

3) *Phase-lag index*: The Phase-Lag Index (PLI) [17] of two signals is defined as

$$PLI(\hat{\mathbf{x}}_i, \hat{\mathbf{x}}_j) = |\langle \text{sgn}(\phi_{\hat{\mathbf{x}}_i}(t) - \phi_{\hat{\mathbf{x}}_j}(t)) \rangle|, \quad (20)$$

i.e. the magnitude of the average over time of the signed values of differences of the instantaneous phases of the signals.

Depending on the application, the temporal connectivity function for phase-based connectivity indexes could be the sign of the phase difference of the signals:

$$\varphi(\hat{x}_i(t), \hat{x}_j(t)) = \text{sgn}(\phi_{\hat{\mathbf{x}}_i}(t) - \phi_{\hat{\mathbf{x}}_j}(t)), \quad (21)$$

or simply the phase difference:

$$\psi(\hat{x}_i(t), \hat{x}_j(t)) = \phi_{\hat{\mathbf{x}}_i}(t) - \phi_{\hat{\mathbf{x}}_j}(t). \quad (22)$$

Because of the negative symmetry of these functions, the total energy of the system at time  $t$  is

$$\begin{aligned} E(G) &= \sum_{i,j} w_{ij} \varphi(\hat{x}_i(t), \hat{x}_j(t)) \\ &= \sum_{i < j} w_{ij} (\varphi(\hat{x}_i(t), \hat{x}_j(t)) - \varphi(\hat{x}_j(t), \hat{x}_i(t))) = 0. \end{aligned} \quad (23)$$

However, summing over a subset of these elements, for example, only over those edges relating to a given node or subset of nodes, would reveal the strength and general nature of the node(s) to lead (+ve) or lag (-ve) in the network at the given epoch. We will now apply these temporal connectivity functions to several simulated and real datasets to provide document of their usefulness.

### III. METHODS

We demonstrate temporal connectivity in simulations and real data sets. The Kuramoto model [19] is used as a simulation to assess the usefulness of temporal connectivity over a layered-graph approach. To test the effectiveness of temporal network clustering coefficient metric (11), we devise a simple regime to detect a spheroid travelling over a 3D grid. We then apply our techniques to real high complexity datasets of international trade and EEG brain functional connectivity to provide evidence of the improvements delivered by a temporal connectivity approach. Specifically with the EEG example we seek to provide applicative evidence regarding the benefits of our approach over a multi-layer graph approach as well as over unweighted temporal connectivity functions.

#### A. Kuramoto Model

We use Kuramoto models to generate six-channel multivariate signals with determined coupling. We use the similar parameters for our model as in [18]. We solve the Kuramoto model of the equations [19]:

$$\frac{d\theta_i}{dt} = \omega_i + \frac{K}{n} \sum_{(i,j) \in \mathcal{E}} \sin(\theta_j - \theta_i), \quad (24)$$

where  $\omega_i$  is the ‘natural frequency’ of channel  $i$ ,  $\theta_i(t)$  is the phase of channel  $i$  at time  $t$  and  $K$  is the coupling strength of the model [19]. By solving this ordinary differential equation, we get the phases of the channels at time  $t$ . We solve for an epoch of length 5000 units with a time-step of 0.1 units. This allows a long enough period for metastability of the system to be reached. We then generate the signals appropriately as  $\mathbf{x}_i = \cos(\theta_i)$  [18].

In order to introduce small epochs of differing activity within these signals, as is of interest to our theory, we perform a piecewise solution to this equation relating to epochs of stronger/weaker synchronisation dictated by coupling strength,  $K$ , as:

$$K = \begin{cases} K_1, & t \in [t_0, t_a] \\ K_2, & t \in [t_a + \Delta t_a, t_b] \\ K_1, & t \in [t_b + \Delta t_b, t_{max}], \end{cases} \quad (25)$$

with initial conditions  $\theta_i(t_a)$  and  $\theta_i(t_b)$ , corresponding to epochs dictated by coupling strengths  $K_2$  and  $K_1$  (the second time), respectively, taken from the solution in the previous epoch.

In our study, the natural frequencies,  $\omega_i$ , are realisations of the random variable  $\omega \sim \mathcal{N}(0, \sigma^2)$  for some suitably chosen  $\sigma$ . It is known that the critical coupling strength for a metastable state is

$$K_c = \frac{2}{\pi f_\omega(0)} \quad (26)$$

where  $f_\omega$  is the probability density function of the natural frequencies. Therefore we define the coupling strength of periods  $[t_0, t_a]$  and  $[t_b + \Delta t_b, t_{max}]$  at the critical point:

$$K_c = K_1 = \frac{2\sqrt{2\pi}\sigma}{\pi}. \quad (27)$$

Where  $\sigma$  is the standard deviation of the distribution of  $\omega$ . We draw mean natural frequencies,  $\bar{\omega}_i$ , from a Gaussian distribution,  $\bar{\omega} \sim \mathcal{N}(0, \sigma_1^2)$ . We enact this simulation over 100 iterations, where the natural frequencies are subject to additive white Gaussian noise, i.e.  $\omega_i = \bar{\omega}_i + \xi_i$ , where  $\xi \sim \mathcal{N}(0, \sigma_2^2)$ . Thus, in fact, from the properties of the sum of two Gaussian distributions,

$$\omega = \bar{\omega} + \xi \sim \mathcal{N}(0, \sigma_1^2) + \mathcal{N}(0, \sigma_2^2) \equiv \mathcal{N}(0, \sigma_1^2 + \sigma_2^2). \quad (28)$$

For our study, we choose  $\sigma = \sqrt{0.5^2 + 0.05^2}$  which gives  $K_1 = K_c \approx 0.8019$ . Therefore we contrast two sets of signals where this coupling is increased to  $K_b = 2$  and decreased to  $K_b = 0.25$  in the epoch  $[t_a + \Delta t_a, t_b]$  (25). By doing this we seek to analyse the difference in response of the system when the coupling strength is set to sub-critical and hyper-critical states in a short epoch.

We repeat this whole process 50 times for newly chosen  $\bar{\omega}_i$ . The initial phases  $\{\theta_i(0)\}_{i=1}^6$  are randomised uniformly over  $[0, 2\pi]$  each time a signal is generated.

For analysis, we choose epochs  $\tau = [t_a, t_b]$  of lengths 30, 75, 150, 300 and 600 to account for relevance of window size on coupling strength change. We compare the reliability of temporal connectivity with a time-layered graph approach where temporal connectivity is computed for disjoint windows of relevant signals of length  $t = 30, 75, 150, 300$  and 600, where  $t \leq \tau$ , over a weighted adjacency matrix computed from the total epoch,  $\tau$ . The time-layered graph approach, on the other hand, computes weighted adjacency matrices for the signals of length  $t = 30, 75, 150, 300$  and 600. Thus the comparison is underpinned by the windows of length  $t$ .

The Kuramoto models, as generated above, are downsampled by a factor of 25. We bandpass the signals with an order 30 FIR filter between 1/30 and 1/3 samples per unit, based on trial and error suitability for the generated signals. The time,  $t_a$ , at which coupling changes is set at 3000 and we study this for instances in which this change lasts for 30, 75, 150, 300 and 600 units. We create graphs of connectivity from the signals and compute average temporal connectivity over three epochs after onset of coupling strength change:  $E_1 = 0 - \tau$ ,  $E_2 = \tau - 2\tau$ ,  $E_3 = 2\tau - 3\tau$ . Thus  $E_1$  relates to the entire epoch in which the changed coupling strength is activated and  $E_2$  and  $E_3$  relate to equally lengthed epochs when the coupling strength reverts back to the critical value (27).

### B. Spheroid travelling on a grid

We construct a  $10 \times 10 \times 10$  grid in Euclidean space where each point corresponds to time-series, as in section II-A1. A weighted connectivity graph is formed from the inverse distance, computed as  $w_{ij} = \exp(-d_{ij}^2/4)$ , between the intersecting points in the grid and amplitudes are distributed normally at random to the vertices as  $\mathcal{N}(0, 0.1)$ . At time  $t$ , the amplitude at vertex  $i$  is increased arbitrarily by an amount,  $s$ , and amplitudes at those vertices one unit away from  $i$  are increased by  $\frac{3}{4}s$ . At time  $t+1$ , again amplitudes are assigned uniformly at random but one of the vertices assigned  $\frac{3}{4}s$  increased amplitude at time  $t$  is now randomly selected for an  $s$  amplitude increase and its closest neighbours are now assigned  $\frac{3}{4}s$ . We can liken this to a spheroid travelling randomly across a grainy image. This process continues for 1000 time steps for values of  $s$  ranging from 0.1 in steps of 0.1 up to 0.9. We then compute the SF graph,  $\bar{\Delta}$ , using weights:

$$\hat{w}_{ij} = w_{ij} \frac{x_i(t) + x_j(t)}{2}, \quad (29)$$

so that higher amplitudes close together produces highest connectivity, and calculate the weighted clustering coefficient,  $C_D$ , at each node at each point in time. The task is then to detect the movement of the spheroid. We compare with simply choosing the vertex with highest amplitude and also by implementing graph filtering

approaches based on the graph adjacency matrix [7] and the graph Laplacian [6]. That is, at time  $t$ , we select the highest value of the vectors  $\mathbf{W} \cdot \mathbf{X}(t)$ ,  $\mathbf{L} \cdot \mathbf{X}(t)$  and also the cubed versions  $\mathbf{W}^3 \cdot \mathbf{X}(t)$ ,  $\mathbf{L}^3 \cdot \mathbf{X}(t)$  to compare a simple temporal connectivity approach with some standard GSP approaches.

### C. Real-world datasets

1) *International Goods and Trades*: The quarterly goods and trades of the countries of the world was gathered from the International Financial Statistics of the International Monetary Fund [20]. We use the data of the first 21 months beginning from January 2014 since this period allows for a good balance between the number of countries included and robustness of connectivity estimation, given that countries which have any missing entries over the chosen period are excluded. Using a temporal connectivity approach here, we hypothesise that by adjusting zero-averaged economic output (14) via pairwise correlations of the data, as in [5], we can explore how a greater integration with the global system promotes economic growth. We thus analyse the node gradients,

$$\sum_j w_{ij} \theta(\hat{x}_i(t), \hat{x}_j(t)), \quad (30)$$

for each country,  $i$ , as it changes over time as well as the average over time. Further, by looking at the variance of the node gradients over time we seek to ascertain the temporal variability of the integrated economic output.

2) *EEG data*: We study an eyes-closed, eyes-open dataset of 129-channel EEG activity. This dataset is available online under an Open Database License from the Neurophysiological Biomarker Toolbox tutorial [21]. It consists for 16 volunteers and is down-sampled to 200Hz. We used the clean dataset which we re-referenced to an average reference and filtered in Alpha (8-13Hz) before further analysis. Alpha activity is well known to undergo notable changes between these states [22], thus such a dataset provides a straightforward testing ground for our techniques on complex brain recordings.

These long recordings allow us to arbitrarily take windows starting at the 1000th sample and lasting 16, 32, 64,  $\dots$ , 4096 samples. We take this measure to avoid the possibility of pre-processing artefacts at the beginning of the signal. To investigate frequency-based dynamics, we compute coherence and PLI for these datasets and choose modules for analysis based on observable differences in the average weights over graphs computed from the largest window-4096. Modules allow us to compute our phase-based methods without redundancy (23). Figure 1 shows these average adjacency matrices. Clearly, around 1-30 nodes and 60-90 nodes both show differences in coherence and PLI, thus we choose these as Module A and Module B, respectively, to compare our methods. Taking modules as opposed to using global connectivity will help us to assess signed-phase temporal connectivity for the PLI.

Modular connectivity is computed as per the formula in [5]:

$$\sum_{t \in T} \sum_{i \in \mathcal{V}_x} \sum_{j \in \mathcal{V}} w_{ij} \mathcal{F}(\hat{x}_i(t), \hat{x}_j(t)), \quad (31)$$

where  $\mathcal{V}_x$  are the module vertices and  $T$  is the epoch of interest. For this dataset we seek to clarify not only the usefulness of our methods compared to weighted graphs by themselves, as in the Kuramoto example, but also the usefulness of temporal connectivity functions with a graph support as opposed to using unweighted temporal connectivity functions, i.e. putting all weights equal 1 in (31).

## IV. RESULTS

### A. Kuramoto Model

We look at the correlation coefficient with both squared difference (14) and instantaneous correlation (17); coherence with instantaneous amplitude difference (19) and PLI with weighted unsigned instantaneous phase difference (21) (unsigned is chosen to avoid redundancy for global measurements). We do paired  $t$ -tests on the values:

$$\sum_{j=1}^n w_{ij} \mathcal{F}(\hat{\mathbf{x}}_i(E_k), \hat{\mathbf{x}}_j(E_k)), \quad (32)$$

for each epoch  $E_k$  separately, where  $\mathcal{F}$  is the relevant temporal connectivity function in section II-D. We compare this with the mean weight alone of graphs computed from different lengths of time windows 30, 75, 150, 300 and 600 units, as for the temporal connectivity.



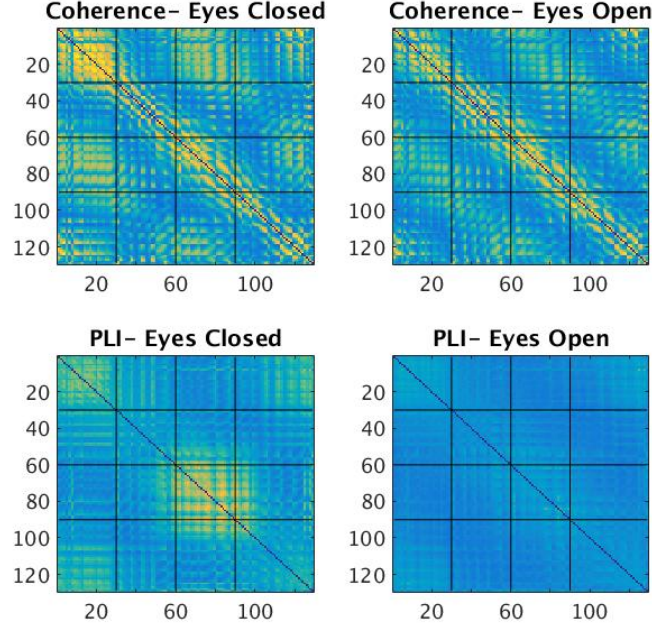


Fig. 1. Weighted graph adjacency matrices of coherence (top) and PLI (bottom) for eyes closed (left) and eyes open (right) conditions. The colour axes, yellow being the largest weights, are the same for eyes open and eyes closed conditions. Modules are selected based on the most different activity between conditions- Module 1: nodes 1-30, Module 2: nodes 60-90, indicated by the black lines.

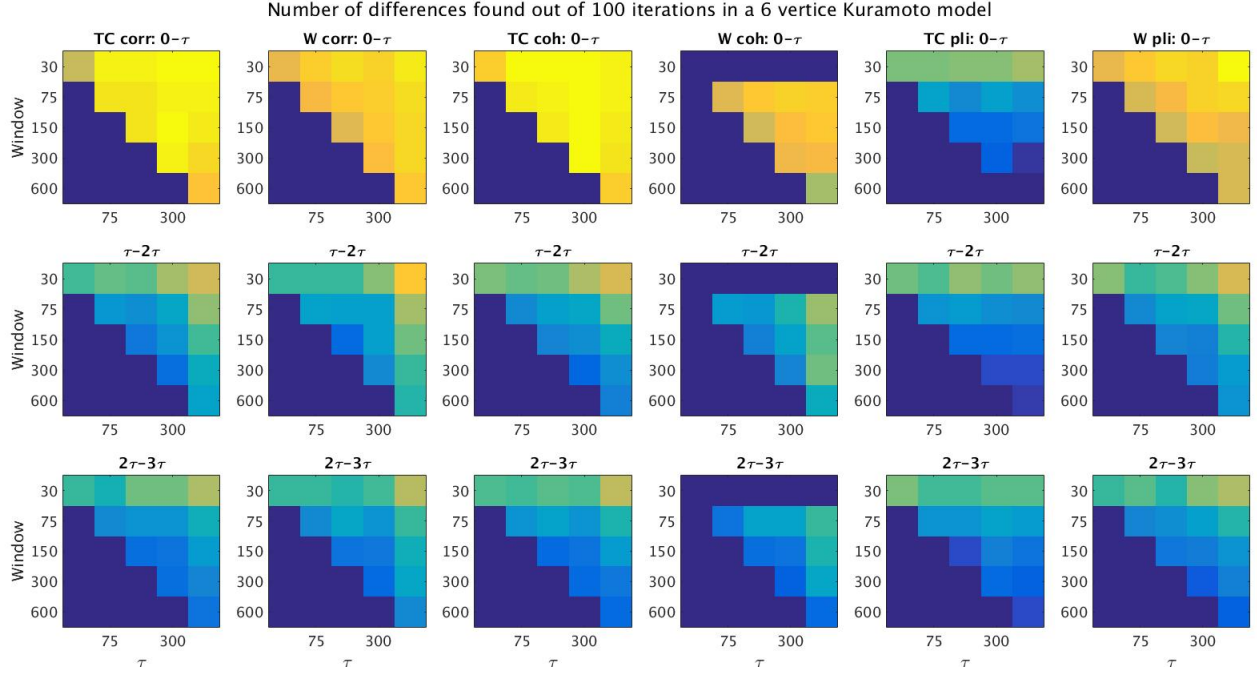


Fig. 2. Number of differences as colour plots with a colour axis from 0 (dark blue) to 100 (bright yellow). Each plot provides the results for each length,  $\tau$ , for the period of difference in coupling between Kuramoto models (y-axis) and each time window taken for temporal connectivity (TC) analysis. Here, 'corr' refers to correlation, 'coh' to coherence and 'pli' to phase-lag index. The first row shows results for period  $0-\tau$ , i.e. the actual active window of different coupling strength. The second and third rows shows control results for the subsequent two windows ( $\tau-2\tau$  and  $2\tau-3\tau$ ) of equal length after the event. Columns 1 and 2 provides results for correlation TC and edge weights, respectively; columns 3 and 4 for coherence TC and edge weights; columns 5 and 6 for pli TC and edge weights.

The number of trials per epoch in which the  $t$ -tests showed significant values is shown in a colour chart (dark blue to bright yellow) in Fig. 2.

It is clear that the unsigned temporal connectivity approach with PLI is not effective in this instance. Since signed

TABLE I

AVERAGE GREATER NUMBER OF INSTANCES OF SIGNIFICANT DIFFERENCES FOUND ( $\alpha = 0.05$ ) BETWEEN COUPLING STRENGTHS  $K_2 = 0.25$  AND  $K_3 = 2$  IN PAIRED  $t$ -TESTS. INSTANCES OVER WHICH AVERAGE NUMBER AND  $p$ -VALUES FROM PAIRED  $t$ -TESTS ARE TAKEN ARE EACH COMBINATION OF  $\tau$  AND ASSOCIATED POSSIBLE TIME WINDOWS. LEGEND: E1 -EPOCH IN WHICH COUPLING STRENGTH IS CHANGED; TC- TEMPORAL CONNECTIVITY; W- TIME-LAYERED GRAPH; CORR- CORRELATION (AND INSTANTANEOUS); SQD- SQUARED DIFFERENCE; COH- COHERENCE; AMP- INSTANTANEOUS AMPLITUDE.

E1	Mean difference	$p$ -value
TC corr > TC sqd	16.8	$1.419 \times 10^{-4}$
TC amp > TC corr	2.4	0.034
TC corr > W corr	7	$5.4207 \times 10^{-4}$
TC coh > W coh	15.733	$7.223 \times 10^{-6}$

weights are always zero for global results, we shall test their effectiveness in the analysis of larger EEG networks where useful subsets of vertices are easier to identify. We note that coherence was unable to be computed for windows of size 30 (12 samples) because the number of frequency points analysed must be less than the number of samples, whereas using temporal connectivity there is no problem with analysis of such small windows. Otherwise, comparing correlation and coherence it appears that the temporal connectivity approach is more effective than the time-layered graph approach, notice the brighter yellow pixels.

To confirm this statistically, we vectorise the results for each  $\tau$  and  $t \leq \tau$ . Table I provides information for the mean of the differences of these vectors for correlation and coherence, i.e. mean of correct differences found for temporal connectivity – time-layered graph. We also perform paired  $t$ -tests on these vectors to show the statistical significance of the mean difference. Also shown in this table are the results for the instantaneous correlation – squared difference for the temporal connectivity with correlation graphs. The squared difference results are thus not presented in Fig. 2 as it is clear that instantaneous phase performs much better (Table I first row). The third and fourth rows show that temporal connectivity is more accurate than the graph layered approach, even when the window for graph construction of temporal connectivity is always taken as the largest possible in our set-up. The second row dictates that the coherence method slightly betters correlation, which is sensible from the frequency-based formulation of the simulations.

### B. Spheroid on a 3D-grid

We take the largest  $C_D$  (11) as the measure to detect the central point of the spheroid at each point in time and compare with just taking the highest amplitude value of the signal and the highest value of GSP filtered signals  $\mathbf{W} \cdot \mathbf{X}(t)$ ,  $\mathbf{L} \cdot \mathbf{X}(t)$ ,  $\mathbf{W}^3 \cdot \mathbf{X}(t)$  and  $\mathbf{L}^3 \cdot \mathbf{X}(t)$ , see Fig.3. As is notable,  $C_D$  obtains the most correct guesses in every instance. Furthermore, none of the GSP versions perform better than the naive highest amplitude approach when  $s \geq 0.2$ . Since  $\mathbf{W}$  and  $\mathbf{L}$  fair better than their cubic versions, we know that the improvement noted by the clustering coefficient method is not down to the cube of the graph distance information resulting from (11).

An example of how the proposed method is able to correctly identify a spheroid centre which has been incorrectly identified using the highest amplitude is shown in Fig. 4. In this example, the increased amplitude of  $3/4s$  given to one of the nearest vertices, 452, provides a larger overall amplitude to the  $s$  given to the central vertex. By using the SF graph method, however, this error due to noise is corrected since most of the nearest vertices to 452 have a very small comparative amplitude to those of the true centre at 462. We performed  $t$ -tests on the populations of distance to the real central vertex provided by the highest amplitude approach and the signal clustering approach. All comparisons showed greater accuracy in the latter approach with  $p < 1 \times 10^{-25}$  except for the  $s = 0.1$  case for which the  $p$ -value was  $3.57 \times 10^{-4}$ .

### C. Real-world datasets

1) *International Goods and Trades*: Fig. 5 shows the original time-series alongside the graph adjusted time series estimated using the node gradient with correlation and normalised squared difference as the temporal connectivity function. We see a stark contrast particularly for mainland China (green), between the original and adjusted time-series. This suggests to us that perhaps the economy of China is not well integrated with the rest of the world. Indeed, there is a rather obvious anti-correlation between the node gradients of China and, for example, the USA.

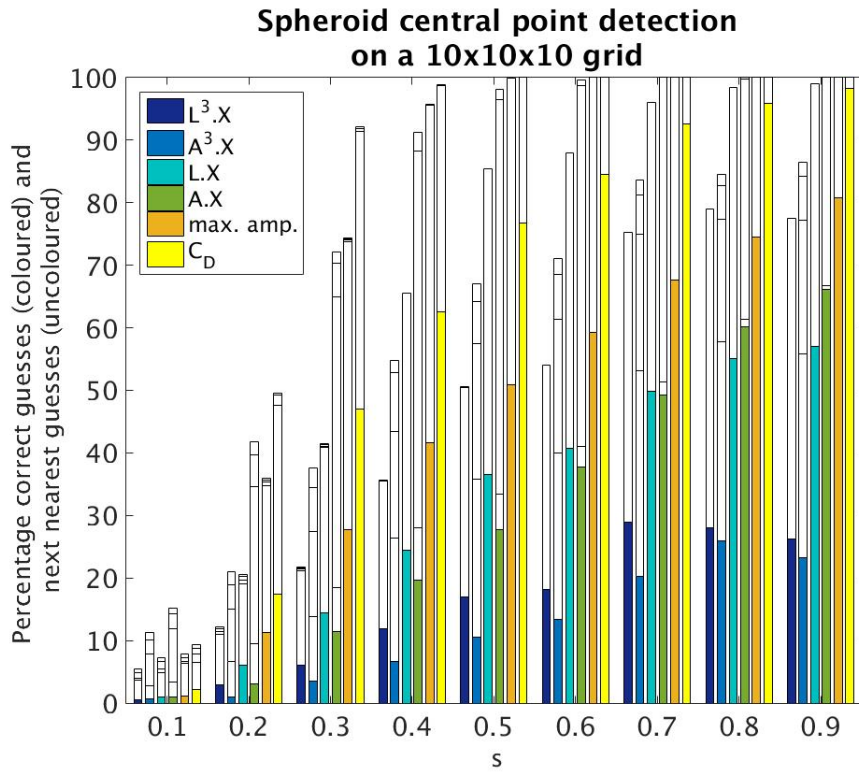


Fig. 3. Percentage of correct (coloured) and next nearest guesses- 1st to 4th nearest vertices, respectively (stacked, uncoloured)- out of 1000 time points using amplitude height only (max. amp.), signal function graph clustering coefficient,  $C_D$  and standard graph signal filtering approaches where  $s$  is the increased amplitude of the central vertex.

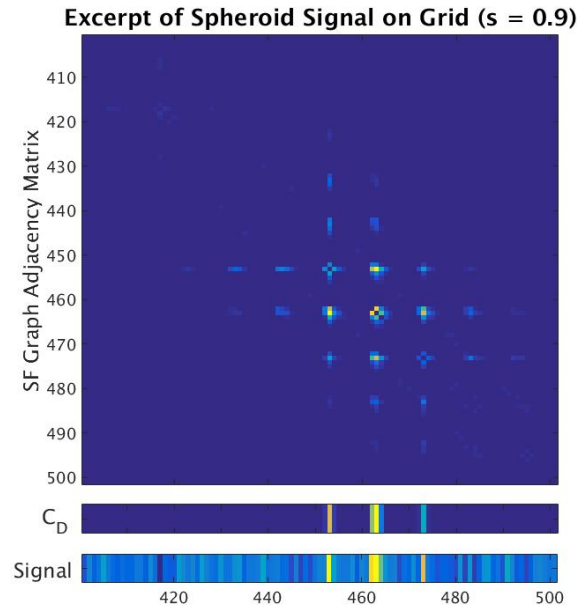


Fig. 4. Example of reduced noise and increased accuracy through SF clustering. The highest amplitude is detected at vertex 452, however the SF Graph clustering coefficient,  $C_D$ , detects the actual centre at vertex 462.

On the other hand the USA (blue) and Germany (red) show a well integrated economy. In fact, Fig. 6 shows the sum of these time series (top) and node gradients (bottom) for each country. We highlight some well known economies. Of all these economies, Germany and USA show a clear dominance in the adjusted version, whereas all the other highlighted economies appear to shrink, gravitating towards the median. Most remarkably, again, is the

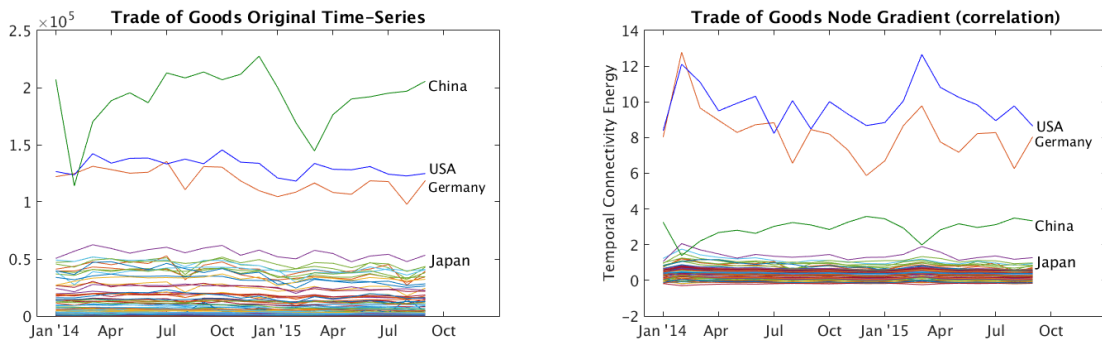


Fig. 5. Left, the quarterly trade of goods (\$) of world countries. We highlight those of China (Mainland), USA, Germany and Japan as the top trading countries in the world. Right, the ‘graph filtered’ signal taken as the node gradient of the given country using the graph of global correlations and the squared difference temporal connectivity function.

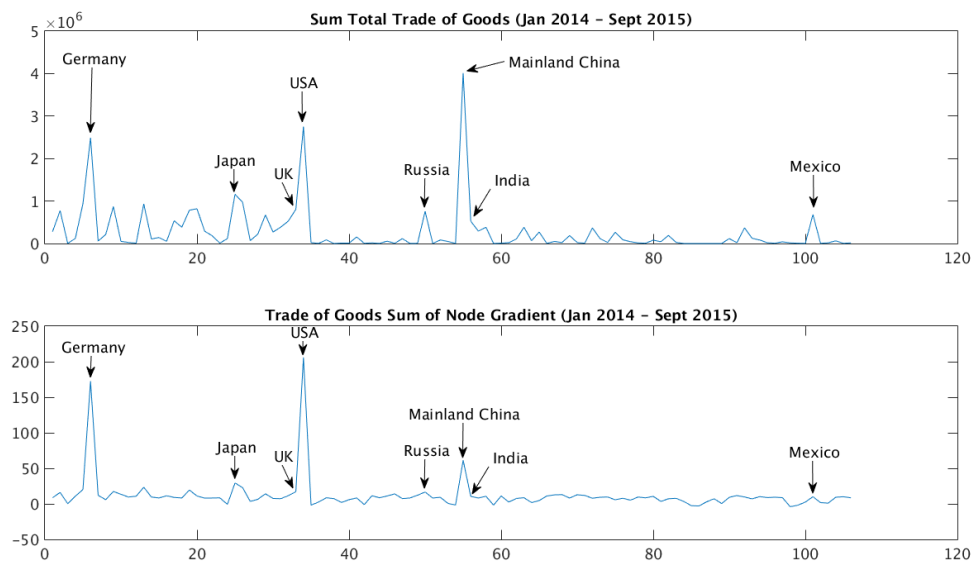


Fig. 6. Top, the total trade of goods (\$) of world countries from January 2014 till September 2015. Bottom, the total of the node gradients of those countries using the graph of global correlations and the squared difference temporal connectivity function.

case of China, which shows a marked shrinking in significance in comparison with the original time-series. Other expectedly large economies, eg. UK, Russia, India and Mexico, largely fail to distinguish themselves from the rest of the world in the adjusted values. Results of standard deviation for the node gradients of Germany (1.4856), USA (1.1834) and China (0.5000) reveal a high variability in Germany and a low variability in mainland China. This contrasts with the much larger variability of the original signal in China than elsewhere (Fig. 5, left). This suggests that the global integration of Germany’s output is rather volatile, whereas the large fluctuations of the original time-series of China appear to be smoothed out when looking at global integration.

2) *EEG data*: For modules A and B similarly as for the Kuramoto model, we compute temporal connectivity using  $\tau$  and  $t \leq \tau$ , all defined in section III-C2. We then compute the density, (differences found)/(total possible) of significant  $p$ -values from paired  $t$ -tests of eyes closed vs eyes open conditions across the 16 participants and plot for modules A and B. For module A, Fig. 7, we see that the temporal connectivity appears the most effective for coherence (column 1), where more yellow means higher percentage of success in finding differences. Particularly, the graphs alone perform poorly in comparison. For PLI, the graphs alone appear most effective in general, whereas the null temporal connectivity (row 2) is particularly poor. In this case, the weighted phase difference is more effective than the unweighted phase difference for temporal connectivity. For module B, Fig. 8, again the temporal connectivity approach appears more effective than the others for coherence (column 1), though notably the graph

### Module A: density of significant $p$ -values

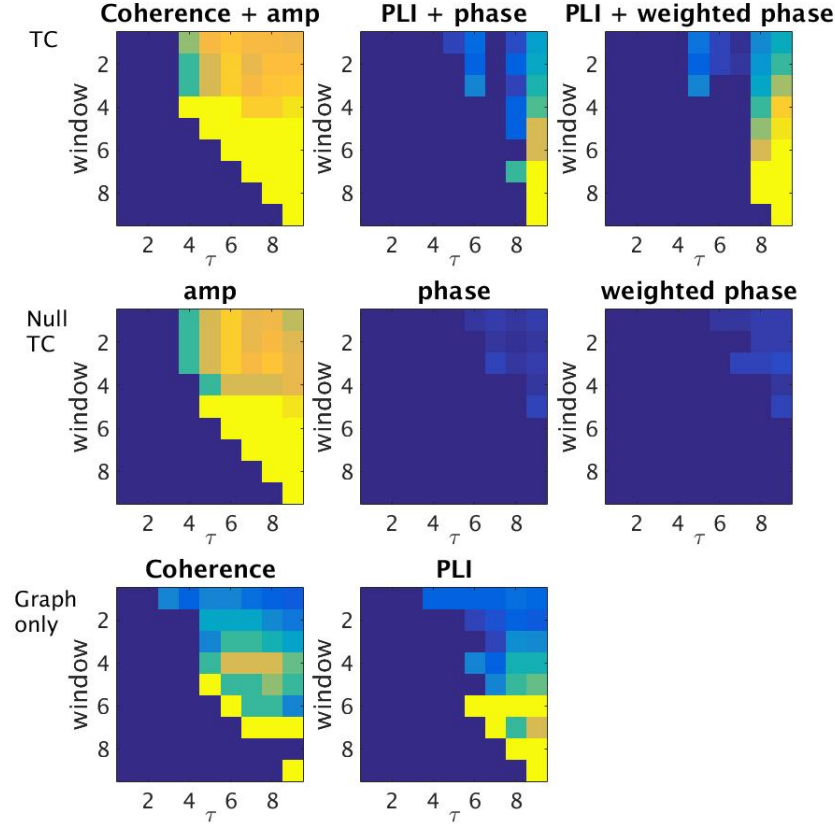


Fig. 7. Module A: Fraction of  $p$  values which are significant for  $\tau$  being the total length of the signal (16,32,64,128,...,4096 samples) and ‘window’ being the computation of the connectivity. TC (first row) is temporal connectivity where the graph comes from  $\tau$  and the TC is computed as per the window. Null TC (second row) is the null temporal connectivity, i.e. not graph weighted. ‘Graph only’ (third row) refers to graphs computed as per the window. Yellow to blue is 1-0 in terms of the density of significant  $p$ -values for the given paradigm.

only approach does considerably better than it does in module A. For the PLI (column 2), we see a contrasting result where the temporal connectivity approach (top) outperforms the graph only approach (bottom). Again here, the weighted phase difference does better than the unweighted case and the null temporal connectivity performs noticeably poorly (second row). It is evident that coherence is in general the better method for establishing the difference between eyes closed and eyes open resting state conditions in this dataset.

We confirm these observations statistically in Table II using an identical approach as for the Kuramoto simulations (Table I), i.e. vectorising the results and calculating mean differences and paired  $t$ -tests for determining the best approach for properties of interest. Particularly, coherence temporal connectivity significantly outperforms the null temporal connectivity and coherence layered graph weights for both Modules (top two rows for modules A and B). In module A it is in fact 20 percentage points clear of the weighted graph approach whilst only 3 percentage points clear of the null connectivity, telling us that the information provided by the null connectivity appears to be the more significant factor here. Rows 3 for A and B show that the weighted phase difference is slightly better than the signed phase difference for PLI temporal connectivity over the two modules, although this is only significant ( $\alpha = 0.05$ ) for module A. Testing which is better between PLI temporal connectivity and the graph only PLI approach, we see that for module A, row 4, there is no significant difference between the two techniques, whereas for module B, row 4, temporal connectivity is clearly more effective by an average of 12 percentage points. Lastly, it is clear that PLI temporal connectivity is more effective than null temporal connectivity for both modules, last two rows for A and B.

### Module B: density of significant $p$ -values

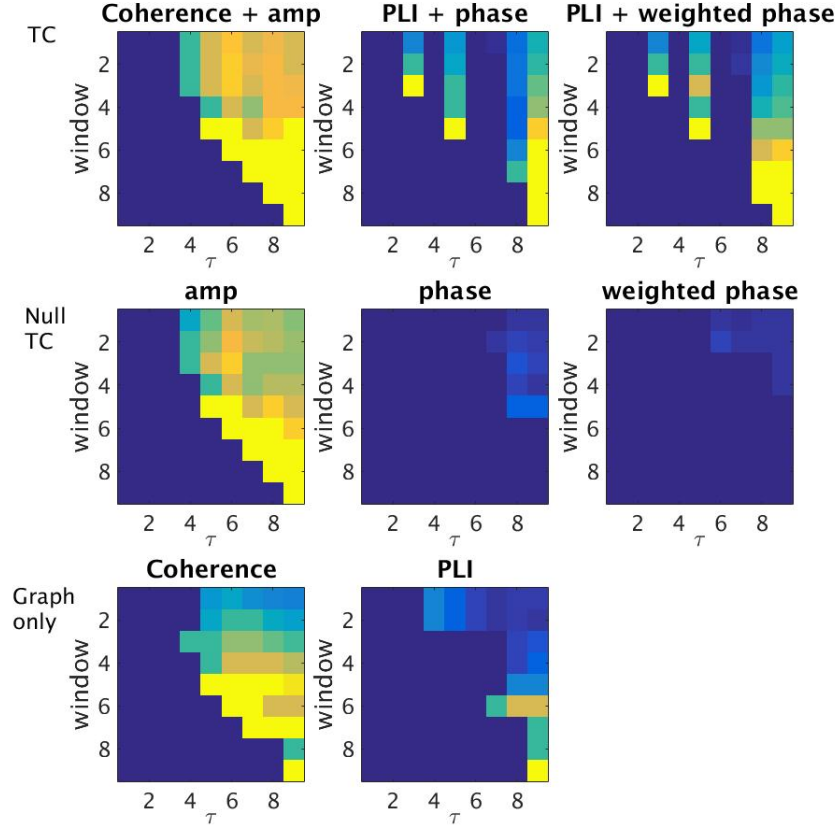


Fig. 8. Module B: Fraction of  $p$  values which are significant for  $\tau$  being the total length of the signal (16,32,64,128,...,4096 samples) and ‘window’ being the computation of the connectivity. TC (first row) is temporal connectivity where the graph comes from  $\tau$  and the TC is computed as per the window. Null TC (second row) is the null temporal connectivity, i.e. not graph weighted. ‘Graph only’ (third row) refers to graphs computed as per the window. Yellow to blue is 1-0 in terms of the density of significant  $p$ -values for the given paradigm.

TABLE II

COMPARING THE DENSITY OF SIGNIFICANT  $p$ -VALUES FOR EEG FUNCTIONAL CONNECTIVITY BETWEEN  $\alpha$  EYES OPEN AND EYES CLOSED RESTING STATE ACTIVITY. LEGEND: ‘PROPERTY OF INTEREST’- VARIABLE(S) LEFT UNCHANGED; ‘COHERENCE’ AND ‘PLI’- GRAPHS USED; ‘AMP’- INSTANTANEOUS AMPLITUDE; ‘PHS’- INSTANTANEOUS SIGN OF PHASE DIFFERENCE; ‘WPHS’- INSTANTANEOUS PHASE DIFFERENCE; ‘TC’- TEMPORAL CONNECTIVITY; ‘NULL’- NULL TEMPORAL CONNECTIVITY; **W**- GRAPH ONLY APPROACH.

Module	Property of interest	Comparison	Mean difference	$p$ -value
A	coherence	TC > <b>W</b>	0.2098	$8.5 \times 10^{-9}$
	amp	TC > Null	0.0332	0.0227
	PLI, TC	wphs > phs	0.0633	0.0018
	PLI	<b>W</b> > TC wphs	0.0084	0.7472
	phs	TC > Null	0.0909	$8 \times 10^{-4}$
	wphs	TC > Null	0.1530	$3.2 \times 10^{-5}$
B	coherence	TC > <b>W</b>	0.1014	$2.7 \times 10^{-5}$
	amp	TC > Null	0.0292	$2.5 \times 10^{-5}$
	PLI, TC	wphs > phs	0.0343	0.0525
	PLI	TC wphs > <b>W</b>	0.1211	$1.8 \times 10^{-4}$
	phs	TC > Null	0.1519	$1.6 \times 10^{-5}$
	wphs	TC > Null	0.1905	$1.6 \times 10^{-6}$



## V. DISCUSSION

The theoretical framework outlined for temporal connectivity provides the connection between the graph and signal domains in a manner which can be readily exploited for a multitude of problems. By defining special operators, we can map linearly between the domains in a meaningful way. Particularly, in the Appendix, equation (37) shows how the Dirichlet energy can be equivalently computed by operating on the edge space or the vertex space and how the Dirichlet graph provides the identity solution in both spaces.

The temporal connectivity technique has been rigorously tested both globally on small sized simulations, showing an improvement in accurately detecting significant coupling changes of signals beyond standard functional connectivity approaches for correlation and coherence, and locally on larger more complex EEG data, again outperforming standard functional connectivity, but also non-graph filtered temporal connectivity. It is reasonable to suggest that this improvement is, in effect, due to a filtering of pairwise signal interactions by suppressing connections deemed unimportant and emphasising those which are most important. That is, we denoise the dynamics. Similarly, computing graphs from short-term windows make those graphs subject to the highly volatile fluctuations of the EEG activity and, thus, less reliable.

Applications to understanding brain function is particularly noteworthy as shown in our previous EEG study where we were able to pinpoint temporal dynamics of task related ERPs to 20ms precision [5] with a very basic approach. Since brain functional connectivity is proposed to be underpinned by synchronisations of electrochemical pulses [23], we expect that applying our methods for frequency and phase-based connectivity measures may even better uncover transient dynamic network activity believed to underlie cognition which, crucially, can aid in clinical neurophysiology such as in understanding and detecting Alzheimer's disease and Schizophrenia [24].

We further explored the flexibility of the theoretical framework for understanding different problems. Using a novel temporo-topological approach, we showed an increased ability to detect a spheroid travelling over a 3D grid over a more naive approach and GSP graph filtering approaches. Based on the assumption of equal radius in all directions of the spheroid, by providing a neighbourhood clustering of the amplitudes, we can better detect where the centre point of the spheroid activity is. Being able to easily manipulate the signal dynamics itself proves to provide a more flexible data analysis method than being restricted to graph adjacency matrix or Laplacian polynomial filters.

Exploring correlations in economic data, we uncovered the fundamental importance of global integration. The two world economic superpowers, USA and China, have drastically different levels of integration with the global system- the former having a long history as an outward-looking proponent of economic liberalism and the latter only recently emerging from economic conservatism [25]. This is clearly reflected in our analysis. However, using the high resolution information from our analysis, we were able to ascertain that China's output was the more stable over time.

Temporal connectivity is a very flexible framework, but this also means that in its application it requires a carefully considered formulation. For example, if one finds that using correlation connectivity weights with a phase-based temporal connectivity function gives the best results, it must be carefully explained why the user believes that this works, given that the components are not directly related. This is the reason that we do not mix these elements in our study and only provide the most obviously meaningful combinations. Since temporal connectivity and time-layered graphs have different frameworks, they may be more useful for different applications which is still to be explored. We hope this theory can be applied to a wide range of datasets and allow users to explore their data networks with power and the highest possible precision.

## VI. CONCLUSION

We provided a general theoretical framework of temporal connectivity. We showed that this framework encompasses graph theory, signal processing and graph signal processing and we provided the link between these domains via an equation relating to the Dirichlet energy of a graph signal. This framework enables temporo-topological analysis at the resolution of the signal of graph connectivity estimated from, e.g., time-series and distances. In simulations we showed that our method using long-term window graph construction with a short-term window analysis is more reliable than using time-layered graphs computed from short-term windows. We further showed that our framework allows the combination of distance with signal information between vertices which outperforms analysis using signals alone both in Kuramoto models and in comparing EEG eyes-open and eyes-closed resting states. In the applied setting, we gathered useful insights into how political realities are reflected in analysis of

economic time-series. The implications of this theory reaches into every domain in which temporal network analysis is desired.

## VII. APPENDIX: DIRICHLET ENERGY EXAMPLE

We take a simple but pertinent example of these theoretical outcomes to explain how Dirichlet energy can be computed equivalently either with vertex-dependent operations, edge-dependent operations or using SF graphs, thus illustrating the validity, generality and broader perspective offered by the proposed theoretical framework.

The Dirichlet energy,  $E(G, t)$ , of graph  $G$  at time  $t$  is

$$E(G, t) = \sum_{i,j=1}^n w_{ij}(\hat{x}_i(t) - \hat{x}_j(t))^2, \quad (33)$$

which measures the inverse smoothness of the vertex weights,  $\hat{\mathbf{X}}$ , at time  $t$  over the edge weights,  $\mathbf{W}$ , [6].

It is known that this can be calculated using graph Laplacian,  $\mathbf{L} = \mathbf{D} - \mathbf{W}$ , of  $G$ , where  $\mathbf{D}$  is the diagonal matrix of the degrees of the vertices in  $G$ . From section II-B4, we see that  $\mathbf{L}$  is the output of an edge-dimension preserving function acting on the edge space. Further, section II-B1 tells us that  $\mathbf{L}$ , with the operation as the usual matrix multiplication,  $\cdot$ , is an operation,  $F_{\mathbf{L}}$ , which can act on the vertex space, i.e.

$$\begin{aligned} F_{\mathbf{L}} : \mathbb{C}^{n \times m} &\rightarrow \mathbb{C}^{n \times m} \\ \mathbf{X} &\mapsto \mathbf{L} \cdot \mathbf{X}. \end{aligned} \quad (34)$$

Symmetrically, we can define a special case  $J$ -matrix as the 3-D matrix  $\mathbf{J} = \{\{x_i(k) - x_j(k)\}_{i,j=1}^n\}_{k=1}^p$ . Then  $F_{\mathbf{J}^\diamond}$  is a function which is dependent on the vertex space and acts on the edge space so that

$$\mathbf{J} \diamond \mathbf{W} = \mathbf{L} \cdot \mathbf{X}, \quad (35)$$

Thus, for  $H = \alpha F + \beta$ ,  $H_{\mathbf{J}^\diamond} \equiv H_{\mathbf{L}}$ , i.e. these functions are equivalent up to linearity. Note that this does not generalise to equivalence with polynomials of the Laplacian,  $\mathbf{L}$ , from which graph signal filters are constructed as in [6]. Clearly,  $F_{\mathbf{J}^\diamond}^2(\mathbf{W}) \neq F_{\mathbf{L}}^2(\mathbf{X})$ - the former is a polynomial of a vertex dependent function while the latter is a polynomial of an edge dependent function.

Finally, we define the Dirichlet SF graph using weights of edge  $(i, j) \in \mathcal{E}$  for  $\{i, j\} \in \mathcal{V}$ , as

$$\hat{w}_{ij}(t) = w_{ij}(x_i(t) - x_j(t)).$$

Analogously to the graph Laplacian in the edge space, we can define the Laplacian of the Dirichlet graph,  $\mathbf{\Gamma} \in \mathbb{R}^{p \times n \times n}$ , of  $G$ , as the output of an edge-dimension preserving function on the graph space, where, taking  $\hat{w}_{ij}(t) = w_{ij}(\hat{x}_i(t) - \hat{x}_j(t))$ ,

$$\mathbf{\Gamma} = F(\{\mathbf{W}, \mathbf{X}\}) = \begin{cases} \sum_{k=1}^n \hat{w}_{ik}(t) & \text{if } i = j \\ \hat{w}_{ij}(t) & \text{otherwise.} \end{cases} \quad (36)$$

We define  $\mathbf{\Gamma}(t)$  as the  $t$ th  $n \times n$  matrix of  $\mathbf{\Gamma}$ . Then, for all  $t$ , the sum of the columns of  $\mathbf{\Gamma}(t)$  is the zero vector,  $\mathbf{0}_n$ , the sum of the rows of  $\mathbf{\Gamma}(t)$  is  $\{2 \sum_{j=1}^n \hat{w}_{ij}(t)\}_{i \in \mathcal{V}}$ , since  $\hat{w}_{ij}(t) = -\hat{w}_{ji}(t)$ , and

$$\mathbf{\Gamma}(t) \cdot \mathbf{1}_n = 2tr(\mathbf{L} \cdot \mathbf{X}(t)).$$

Further, the sum of the diagonal of  $\mathbf{\Gamma}$  is  $\{\sum_{j=1}^n \hat{w}_{ij}\}_{i \in \mathcal{V}}$  so that

$$\mathbf{\Gamma}(t) \diamond \mathbf{I}_n = \mathbf{J} \diamond \mathbf{W}$$

and thus we have the following equivalence:

$$\mathbf{\Gamma}(t) \diamond \mathbf{I}_n = \mathbf{J}(t) \diamond \mathbf{W} = \left\{ \sum_{j=1}^n \hat{w}_{ij}(t) \right\}_{i \in \mathcal{V}} = \mathbf{L} \cdot \hat{\mathbf{X}}(t) = \frac{1}{2} \mathbf{\Gamma}(t) \cdot \mathbf{1}_n. \quad (37)$$



## REFERENCES

- [1] M.E.J. Newman, “Networks”, *Oxford University Press*, UK, 2010.
- [2] A.L. Barabási, “Network Science”, *Cambridge University Press*, UK, 2016.
- [3] P. Holme, J. Saramaki, “Temporal networks”, *Physics reports*, 519(3): 97-125 (2012).
- [4] M. De Domenico, A. Sol-Ribalta, E. Cozzo, M. Kivel, Y. Moreno, M.A. Porter, S. Gmez, and A. Arenas, “Mathematical Formulation of Multilayer Networks”, *Phys. Rev. X*, 3: 041022, 2013.
- [5] K. Smith, B. Ricaud, N. Shahid, S. Rhodes, J. Starr, A. Ibanez, M. Parra, J. Escudero, P. Vandergheynst, “Locating Temporal Functional Dynamics in Visual Short Term Memory Tasks using Modular Dirichlet Energy”, *Scientific Reports*, 7: 42013, 2017.
- [6] D. Shuman, S.K. Narang, P. Frossard, A. Ortega, P. Vandergheynst, “The emerging field of signal processing on graphs”, *IEEE Signal Processing Magazine*, 30(3): 83-98, 2013.
- [7] A. Sandryhaila, J.M.F. Moura, “Discrete signal processing on graphs”, *IEEE Transactions on Signal Processing*, 61(7): 1644-1656, 2013.
- [8] A. Segev, “The node weighted Steiner tree problem”, *Networks*, 17(1): 1-17, 1987.
- [9] A. Sandryhaila, J.M.F. Moura, “Big data analysis with signal processing on graphs: representation and processing of massive data sets with irregular structure”, *IEEE Signal Processing Magazine*, 31(5): 80-90, 2014.
- [10] A. Loukas, D. Foucard, “Frequency Analysis of Temporal Graph Signals”, arXiv preprint arXiv:1602.04434, 2016.
- [11] L. Riu, H. Nejati, N-M. Cheung, “Dimensionality reduction of brain imaging data using graph signal processing”, *IEEE ICIP Conference 2016*, doi:10.1109/ICIP.2016.7532574, 2016.
- [12] S. Sikdar, N. Ganguly, A. Mukherjee, “Time series analysis of temporal networks”, *Eur. Phys. J. B*, 89: 11, 2016.
- [13] Fallani, F.D.V., Richiardi, J., Chavez, M., Achard, S., Graph analysis of functional brain networks: practical issues in translational neuroscience. *Phil. Soc. R. Soc. B*, 369(1653): 20130521, 2014.
- [14] Papo, D., Zanin, M., Pineda-Pardo, J.A., Boccaletti, S., Buldu, J.M., Functional brain networks: great expectations, hard times and the big leap forward. *Phil. Soc. R. Soc. B*, 369(1653): 20130525, 2014.
- [15] F. Schweitzer, G. Fagiolo, D. Sornette, F. Vega-Redondo, A. Vespignani, D.R. White, “Economic Networks: The New Challenges”, *Science*, 325(5939): 422-425, 2009.
- [16] T.S. Rappaport, “Wireless communications: principles and practices”, *IEEE Press*, ISBN: 0-7803-1167-1, 1996.
- [17] C.J. Stam, G. Nolte, A. Daffertshofer, “Phase lag index: Assessment of functional connectivity from multi channel EEG and MEG with diminished bias from common sources”, 28(11): 11781193, 2007.
- [18] B. Lusch, P.D. Maia, J.N. Kutz, “Inferring connectivity in networked dynamical systems: Challenges using Granger causality”, *Physical Review E*, 94: 032220, 2016.
- [19] J.A. Acebrón, L.L. Bonilla, C.J. Prez Vicente, F. Ritort, R. Spigler, “The Kuramoto model: A simple paradigm for synchronization phenomena”, *Rev. Mod. Phys.* 77(137), doi:10.1103/RevModPhys.77.137, 2005.
- [20] International Monetary Fund, Trade of goods dataset: <http://data.imf.org/regular.aspx?key=60998117>, 2016.
- [21] Neurophysiological Biomarker Toolbox, [www.nbtwiki.net](http://www.nbtwiki.net), last visited 8th Sept. 2016.
- [22] R.J. Barry, A.R. Clarke, S.J. Johnstone, C.A. Magee, J.A. Rushby, “EEG differences between eyes-closed and eyes-open resting conditions”, *Clinical Neurophysiology*, 118(12): 2765-2773, 2007.
- [23] C.J. Stam, E.C.W. van Straaten, “The organization of physiological brain networks”, *Clinical Neurophysiology*, 123(6): 10671087, 2012.
- [24] C.J. Stam, “Modern network science of neurological disorders”, *Nature Reviews Neuroscience*, 15: 683695, 2014.
- [25] P. Nolan, “China and the Global Business Revolution”, *Palgrave Macmillan*, UK, 2001.